Southern African Large Telescope

Title:	**Experiment in SALTICAM observing procedures**
Author(s):	**Alexei Kniazev, Petri Vaisanen**
Doc. number:	**2251AC0001**
Version:	**1.2**
Date:	*November 15, 2011*
Keywords:	SALTICAM, RSS, Direct images, Reduction
Approved:	**David Buckley (Ast Ops Manager)**
	Signature:_____ Date:_____

ABSTRACT

We present results of observations with SALTICAM without guiding, but with a dithering pattern and show a method of using such data to build a proper SALTICAM flat-field. We discuss the way of correcting SALTICAM data separately for low-frequency pattern (illumination pattern) and high-frequency pattern (pixel-to-pixel) and show comparisons with SDSS data.

South African Astronomical Observatory, Cape Town 7925, South Africa

Contents

List of Figures

1 Introduction

It is well-known that SALTICAM has very strong vignetting over the field-of-view. This illumination pattern varies with time because the tracker position changes and possibly for other reasons as well. Can any kind of flat-field (sky flats or flats from calibration system) remove these illumination variations over the science field of SALTICAM observations? Previous investigations (Balona, 2007; Loaring, 2006, 2008; Vijay, 2011) have shown poor results when using calibration system flats or twilight flats for this purpose and recommended to use the science data themselves to build a proper flat (Vijay, 2011). How could it be done? Together with SALTICAM guidance problems (guider is located behind of shutter and additionally produces very strong vignetting in case it's used), it is very important to understand the strategy of "normal" SALTICAM observations as well as accuracies of any suggested strategy.

In this report we would like to suggest a way of observations with SALTICAM, which is based on our knowledge of telescope drifts during open-loop tracking and shows the result of such observations. Additionally we can show that data taken in this way could be used for proper data reduction: (1) additional gain correction, (2) correction for illumination variations, (3) correction for pixel-to-pixel sensitivity. We discuss limitations of such method, and suggest more observational strategies to correct for those.

We are going to use these observed and reduced data in follow-up reports, where we are going to present the accuracy and depth of photometry that can be reached with SALT in a reasonable time.

2 Observations and data reduction

The strategy used for the SALTICAM observations presented here was the following:

- To calibrate our final images with proper photometry, we obtained data with SDSS-g and r filters of the field with coordinates RA=05:00:00.0, DEC=00:00:00. This field has a high enough, but not too high, density of stars (see Figure 1) and was observed by SDSS.

- We know from (Kniazev, 2011), that absolute values of X and Y drifts of the telescope essentially do not depend on Azimuth and are in the range of 0.5–0.8 arcsec/min. Taking into account that median seeing (FWHM) for SALT is about 1.3–1.5 arcsec, we used exposure times of 60 sec per frame with 4×4 binning (∼0.55 arcsec/pixel).

- A cycle consisting of 3 frames in g filter and 3 frames in r filter with a subsequent manual dithering of the telescope of approximately 20 arcsec after this step. We planned to take 3 to 5 such cycles to have a possibility to ultimately build a median flat-field.

Our log of observations taken on October 23, 2011, is shown in Table 1. As it is possible to see from this table, we finally were able to observe five cycles. All primary data reduction was done with SALT science pipeline (Crawford et al., 2010).

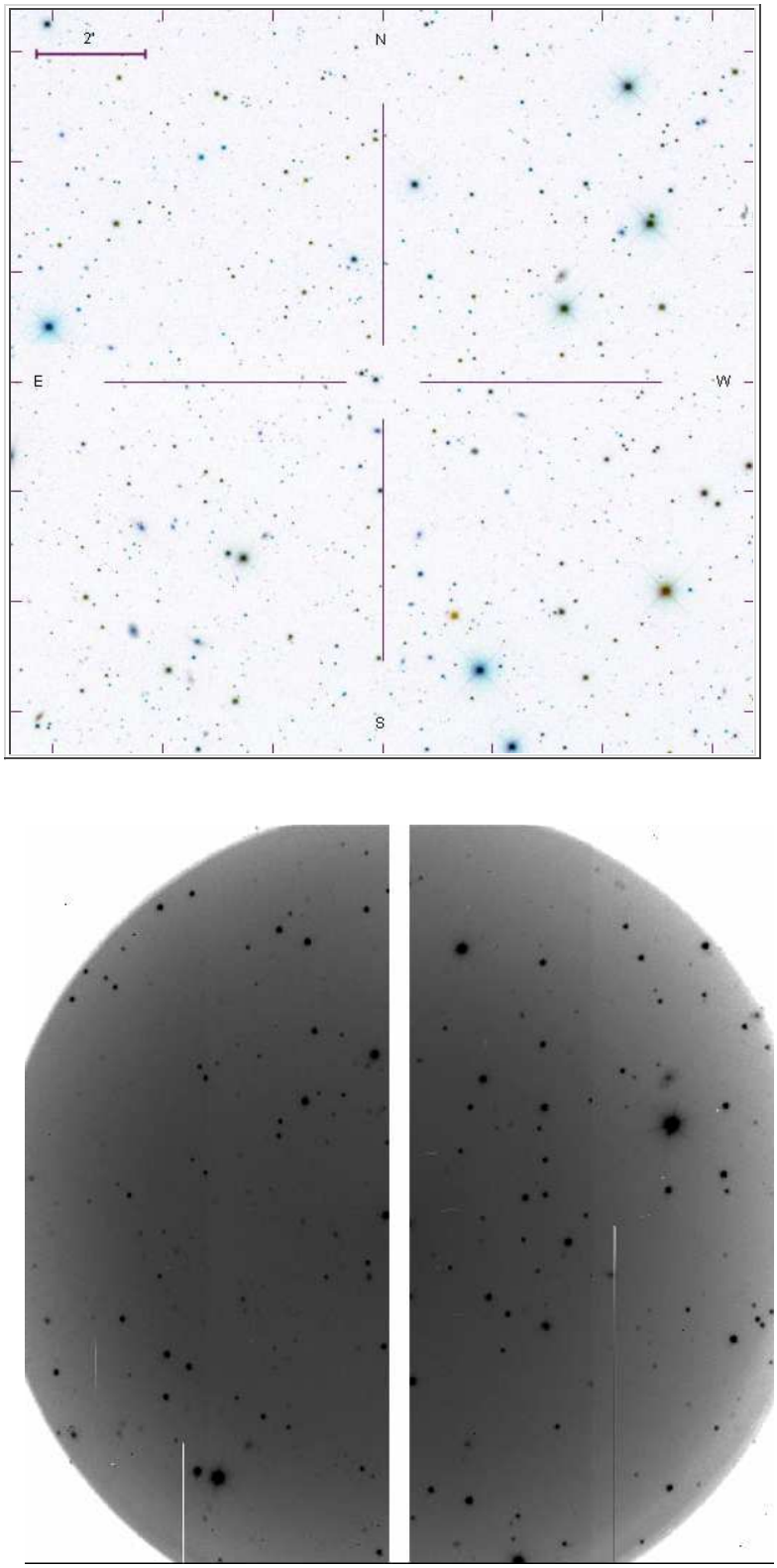

Figure 1: *Top:* The studied field from SDSS (combined *gri* image). Shown size is 13.52×13.52 arcmin. *Bottom:* SALTICAM image of the studied field in *g*-filter. Exposure is 60s.

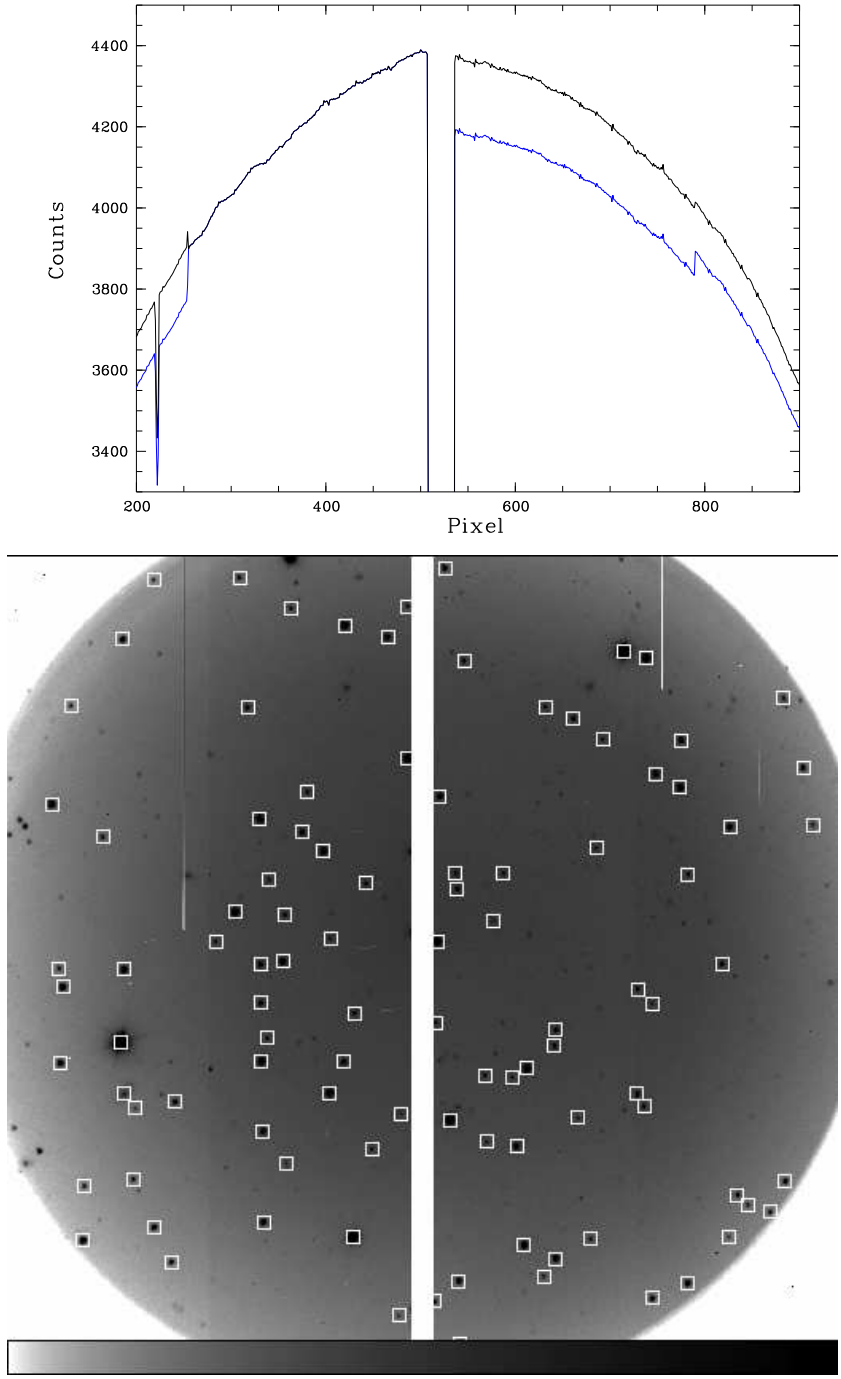

Figure 2: *Top:* The average of 50 central rows before (blue) and after (black) additional gain correction. *Bottom:* Studied field in *g*-filter. All 128 objects which were used to calculate transformation are marked with white squares.

Table 1: Part of Observational log on October, 23d

Image number	Exposure	Filter	Binning	Mode	Comment
S703–705	3×60	sdss-g	4×4	f/f	
S706–708	3×60	sdss-r	4×4	f/f	Dither to 20 arcsec at the end
S709–711	3×60	sdss-g	4×4	f/f	
S712–714	3×60	sdss-r	4×4	f/f	Dither to 20 arcsec at the end
S715–717	3×60	sdss-g	4×4	f/f	
S718–720	3×60	sdss-r	4×4	f/f	Dither to 20 arcsec at the end
S721–723	3×60	sdss-g	4×4	f/f	
S724–726	3×60	sdss-r	4×4	f/f	Dither to 20 arcsec at the end
S727–729	3×60	sdss-g	4×4	f/f	
S731–733	3×60	sdss-r	4×4	f/f	twilight started here.

3 Analysis and Results

3.1 Additional gain corrections

As a first step, our data needed to be corrected for gain in addition to the primary data reduction. The standard SALT pipeline produces a gain correction only with an accuracy of about 3–5% (see top panel of Figure 2).

3.2 X,Y and Rho drifts

To calculate X, Y and Rho (rotational) drifts we used the same method as in Kniazev (2011). 128 stars were selected in each image and a transformation was calculated between each of them and the first frame. Calculated X,Y drifts for the first 6 images (before first dither) are shown in the top panel of Figure 3. The estimated averaged linear drifts are 0.38 arcsec/min for X (RA) and 0.51 arcsec/min for Y (DEC) which are very close to the previously calculated ones (see Figure 4 top panel for the comparison). Calculated rotational drift is shown in the bottom panel of Figure 3. The estimated averaged rho drift is 0.0041 degrees/min, that is also very close to previously calculated for this azimuthal angle (see Figure 4 bottom panel for the comparison).

3.3 Evolution of FWHM during of observations

The evolution of FWHM for taken data is shown in Figure 5. We present here as FWHM the average value of gauss-fit results to all 128 objects, measured for calculations of X,Y and Rho drifts. As it is easy to see from this Figure, after each dither of the telescope, observations had a jump of FWHM value. Within each sequence of 6 frames, the change of FWHM had a much smaller amplitude. The detected PSF elongation is about 10%.

3.4 Problem of flat-fielding

3.4.1 Simple flat-field, based on observed data

To produce a simple flat, based on observed data, we just made a median of all frames observed in a given filter: 15 frames were used in g and 15 frames in r. The resulting flat-field for g-filter is shown in the top panel of Figure 6. It is possible to see some remnants from many different objects even after 15 frames were combined and each set of three were dithered relative to others. These remnants of sources are just a result of the specific median filter size used and the dithering pattern and can be taken care of (see also next Section). The result of correcting the science frames using such a flat-field is shown in the middle panel of Figure 6, where the first and the last observed images are shown. Their 1D profiles are shown in the bottom panel of Figure 6. As mentioned, the artefacts from sources are not a serious issue, but the major issue is the strongly differing larger scale pattern, the shape of the overall sky background.

It is known that for SALT the flat-field low-frequency shape (illumination pattern) is changing continuously, because of the tracker position and possibly other reasons as well. For this reason the result from using such a simple flat-field is far from ideal:

- The final sky background distribution shows up to 15% variations relative to the center ($\sim 25-30\%$ in total) in many frames.
- Even after combining four dithers the final flat image still has some remnants with intensity up to 5-10% of the level of sky background. Their amplitude has a tendency to grow towards the outer parts.

3.4.2 Two step flat-fielding, based on observed data: low-frequency and high-frequency flats

Another idea is to split the flat-field correction into two steps:

- first, to correct each frame for its own illumination pattern, which we are going to build using the frame itself.
- second, use these frames which are now corrected for the illumination pattern to build a high-frequency flat-field to correct for pixel-to-pixel variations.

We created the illumination pattern for each frame using a fast-median algorithm with an aperture diameter of 51 pixels. An example of such an illumination pattern is shown in the top panel of Figure 7 for the first image observed with g-filter. The result of division is shown in the bottom panel of Figure 7. All g or r frames corrected for the illumination pattern were then used to produce a median averaged high-frequency pattern (see Figure 8). This step was done with IRAF `imcombine` task. All g and r frames, finally, were corrected for these high-frequency patterns. Some examples of final frames corrected for both low-frequency and high-frequency flats are shown in Figure 9.

Figure 10 shows the difference in quality between the first method, described in Section 3.4.1 and the current one. With this second method we can guarantee the final flatness of the sky background to be better than 1–2%.

The signal-to-noise ratio for the background (the ratio between level of background and stdev of background pixels in this CCD region) after such a flat-fielding procedure increased up to 10% in the central part of g frames (from 57 to 63) and up to 30–40% for the outer parts (from 34 to 54). For the r frames this increase was from 77 to 89 for the central parts and from 40 to 83 for the outer parts. These results give us hope that the final accuracy of photometry will be very uniform across the field and will not depend on the distance from the centre of the frame.

Finally, note that the resulting flat-fielded frames still have clear artefacts of the objects in the original frames, though they are vastly smaller than e.g. those seen in the middle panels of Figure 6. We believe that these can be removed with more careful steps: e.g. using a varying median filter box size or by using mode in the illumination pattern creation, by never taking more than 1 frame at a given location, by using various SOC algorithms (e.g., Shergin, Kniazev, & Lipovetsky, 1996), and/or a two-step process where detected object pixels are flagged out of the final combination as is commonly done in near-IR sky construction routines. These are details more for the PI to think about, however: here the main interest was to show what kind of observations are needed and what the overall process to derive flat fields are.

3.4.3 Limitations of the method and possible solutions

We will have problems with photometry of extended objects with sizes larger than 1/2 of filter size. For a median filter with aperture of 51 pixel it is >15 arcsec. We can increase the aperture size, but with high probability this will result in problems at the edges. In reality, the filter size has to be selected on the basis of science needs, and the PI of the data will have to determine that. Even more important, the PI will have to be responsible for the optimal dither size for him/her to be able to create the optimal flat field.

One of possible ways to solve the problems with photometry of extended objects are observations where a separate sky-field is taken as part of the dither pattern, with e.g. a 10 arcmin offset, as is commonly used in near-IR observations. Maybe this is a solution, but has to be checked, since SALT illumination pattern could be different for these two positions.

Another good way would be to find a suitable surface model fit for the illumination pattern which would intelligently avoid contamination of even larger sources while still retaining the vignetting pattern differences at sub-arcmin level.

The ideal way, of course, would be to find an analytic expression for the illumination pattern as the function of different telescope and tracker parameters.

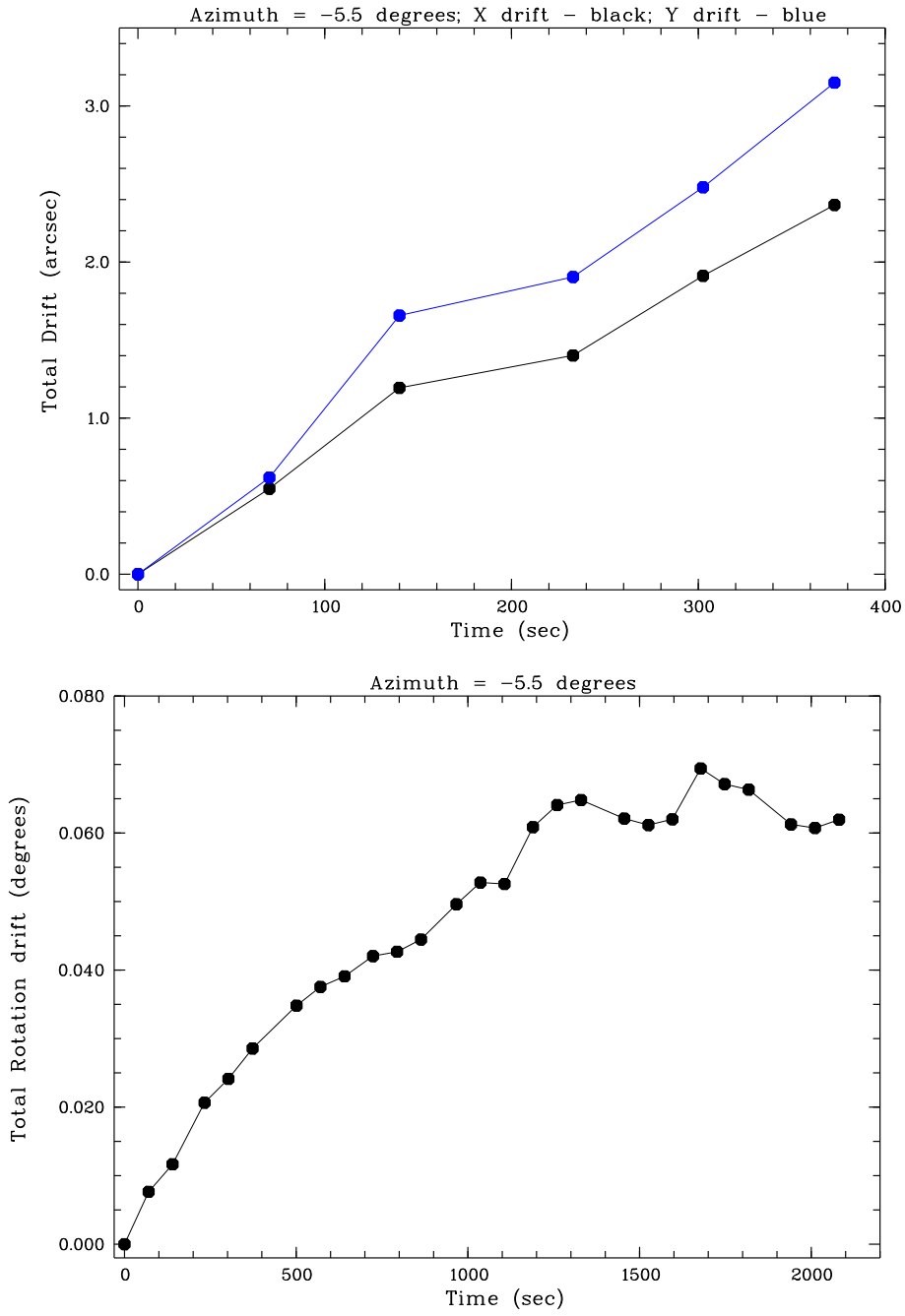

Figure 3: Drifts of the observed field. *Top panel:* Linear X,Y (RA,DEC) drifts of the telescope. X (RA) drift is shown with black dots and Y (DEC) drift is shown with blue dots. Only the first six frames are shown, before the first dither. *Bottom panel:* Rotational drift of the telescope.

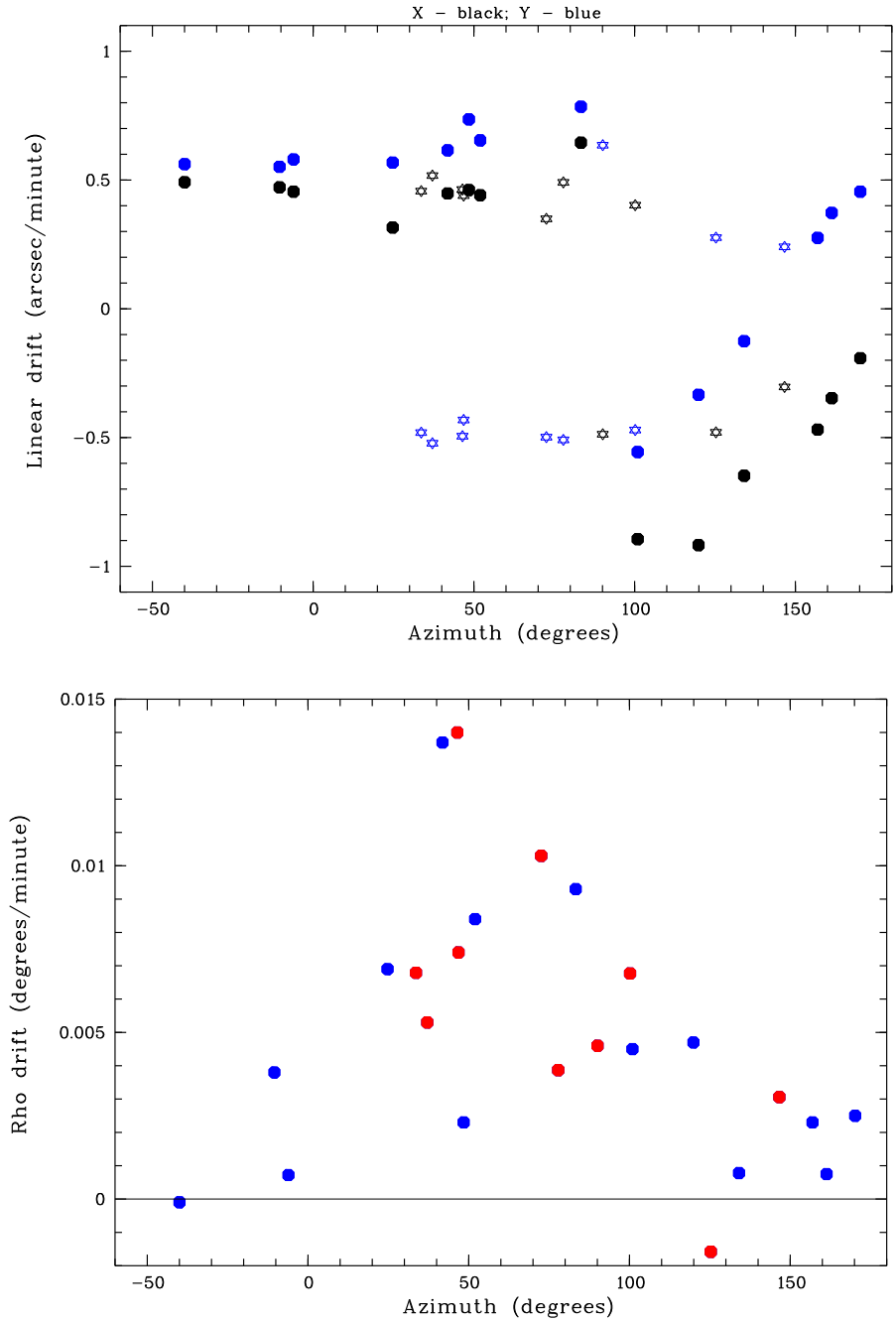

Figure 4: Previous results on drifts of the telescope from Kniazev (2011). *Top panel:* RA and DEC linear drift of the telescope in arcsec per minute depending on azimuth of the telescope and without guiding system. Calculated RA drift is shown with black dots and DEC drift is shown with blue dots. Colored stars shows the same drifts, but after the telescope pointing model was updated (May 2011). *Bottom panel:* Rho drift of the telescope in arcsec per minute depending on azimuth of the telescope. Red dots show drifting after the telescope pointing model update (May 2011).

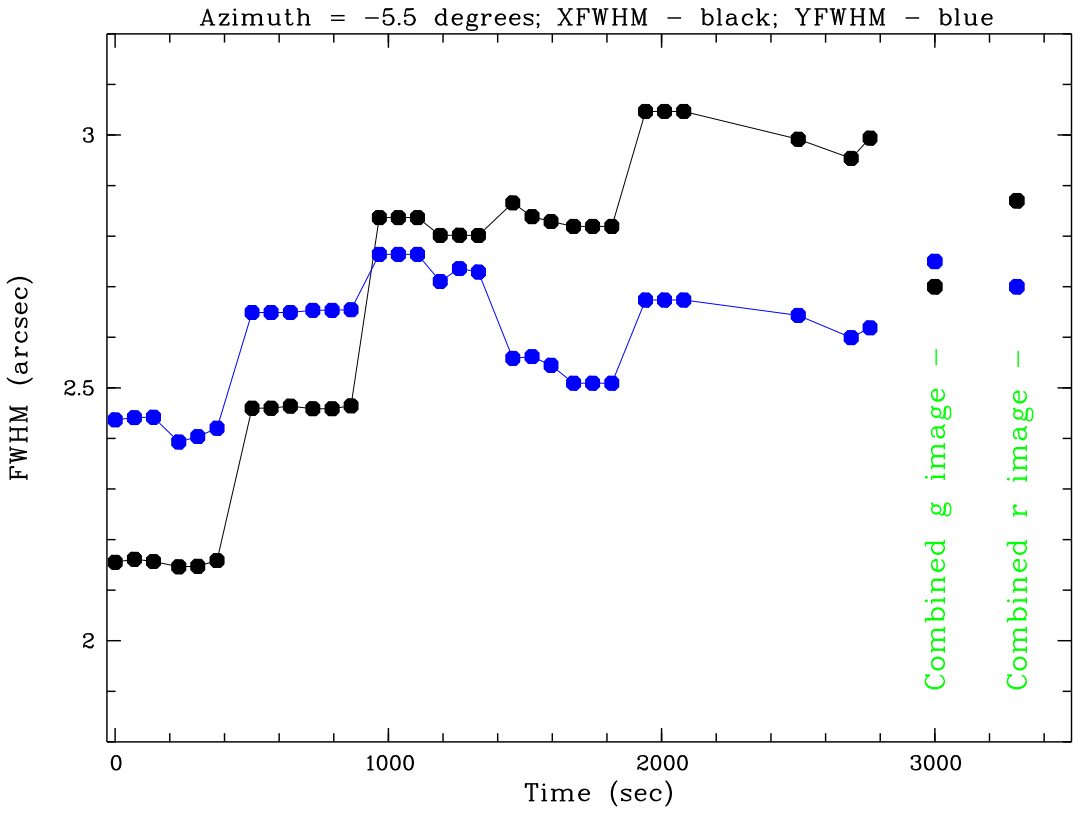

Figure 5: Evolution of average FWHM for studied sources: first three images were observed with g-filter, next three – with r-filter etc. It is easy to see that FWHM value has a jump after each dither of the telescope.

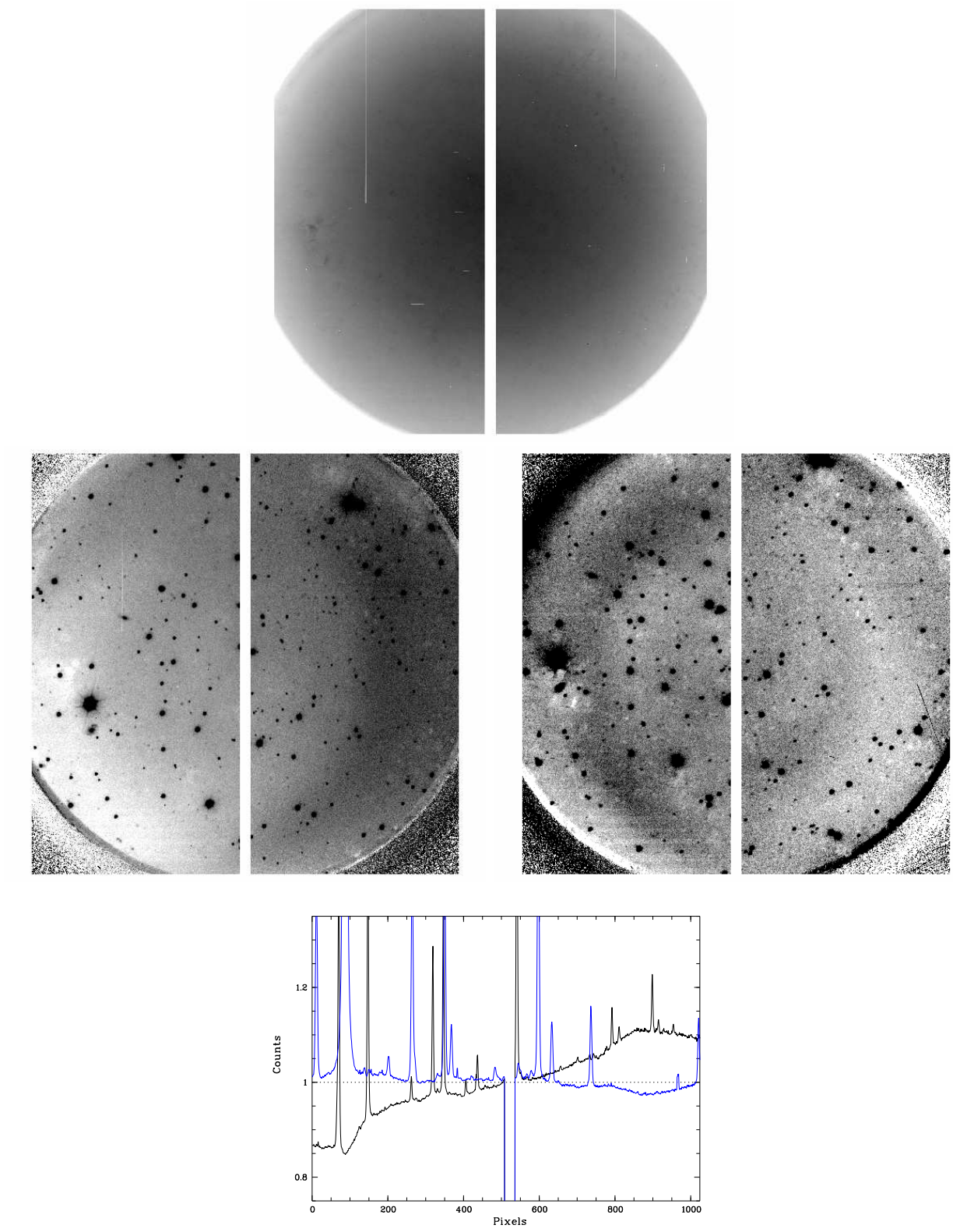

Figure 6: *Top:* The g-flat frame as a result of median average of all g-frames. *Center:* The first and the last g images after they were divided by g-flat. *Bottom:* The average of 50 central rows for the first (black) and the last (blue) g images after they were divided by g-flat.

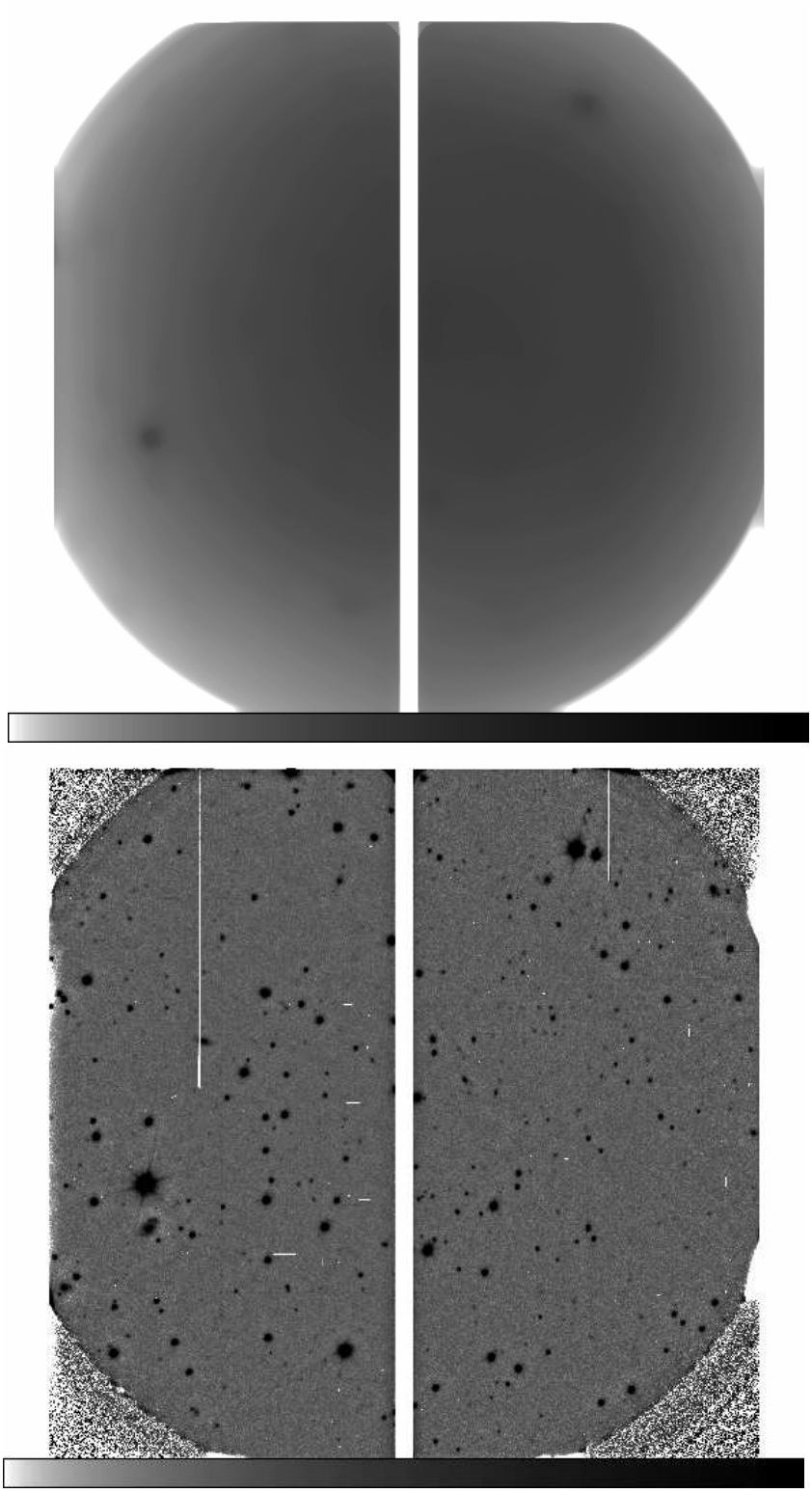

Figure 7: *Top:* The result of fast-median filter with aperture diameter of 51 pixels for the first image taken with *g*-filter. *Bottom:* The result of division of the image to this low-frequency *g*-flat.

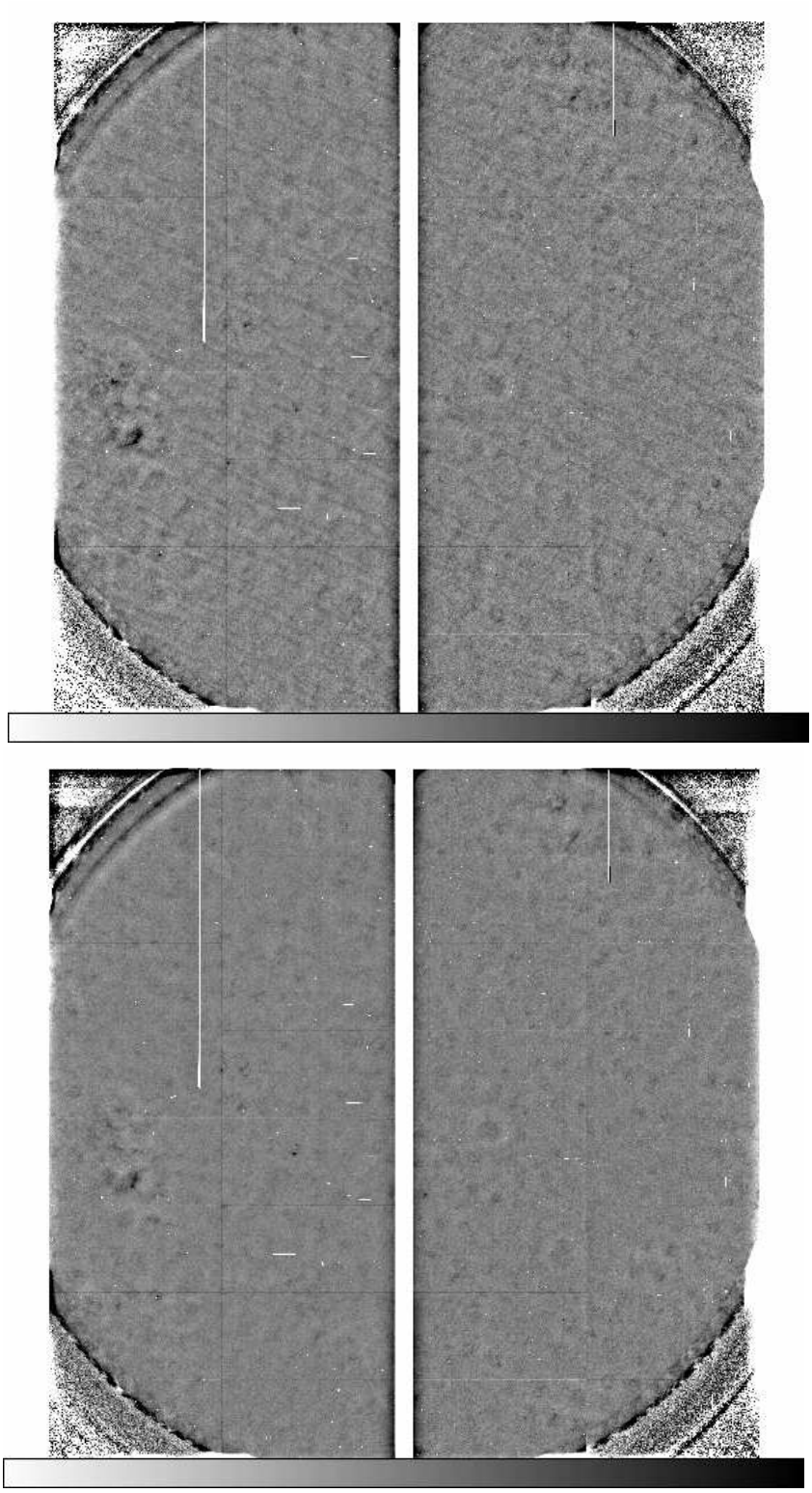

Figure 8: *Top:* The high-frequency g-flat as a result of median average of all g-frames previously corrected for the low-frequency g-flats, which were build for each frame with fast-median filter. *Bottom:* The same, but for the r-filter.

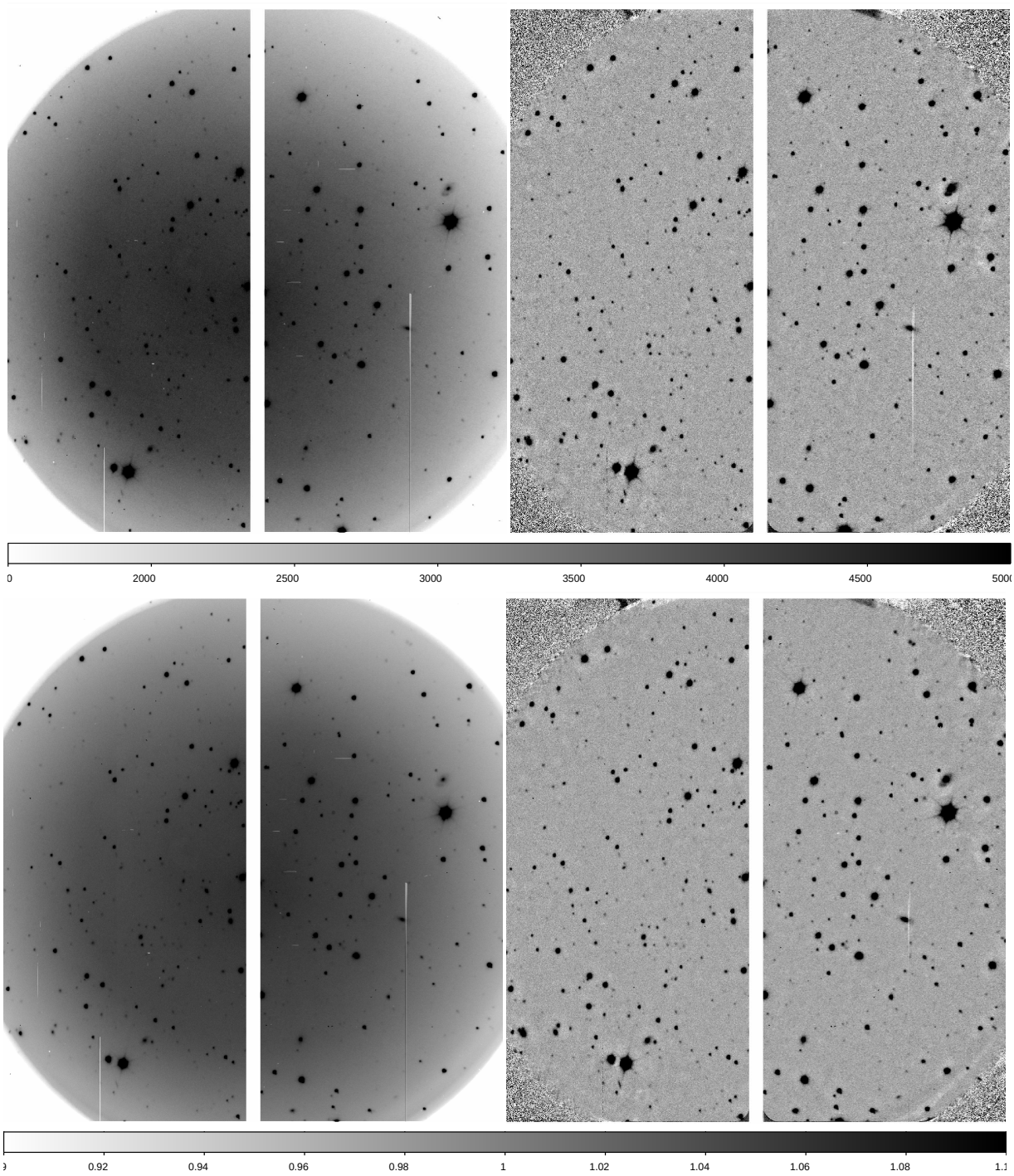

Figure 9: *Top:* The first taken *g*-image after primary reduction and additional gain correction (left panel). The same image, but finally corrected for both low-frequency and high-frequency flats (right panel). *Bottom:* The same, but the first taken *r*-image.

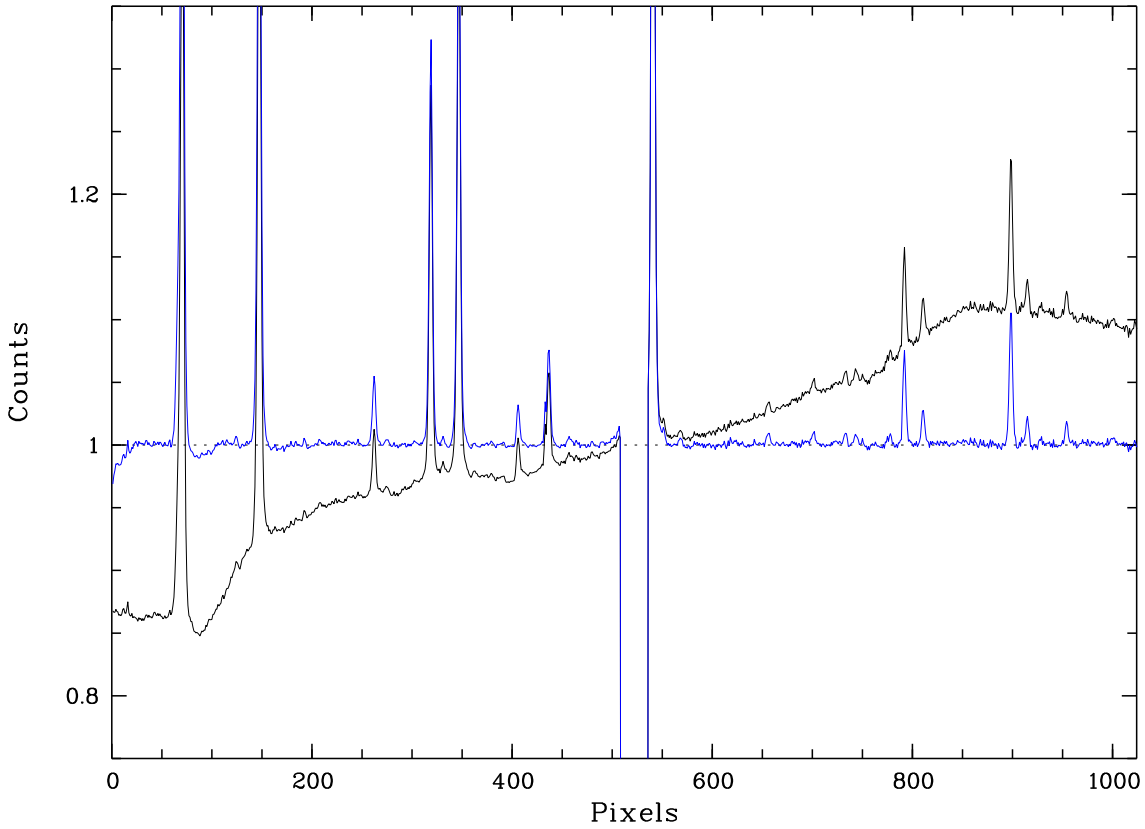

Figure 10: The average of 50 central rows for the first g-image after it was divided with simple g-flat (black) as it was shown in Figure 6 and more accurate case (blue), where low-frequency and high-frequency flats were created separately (top panel of Figure 9).

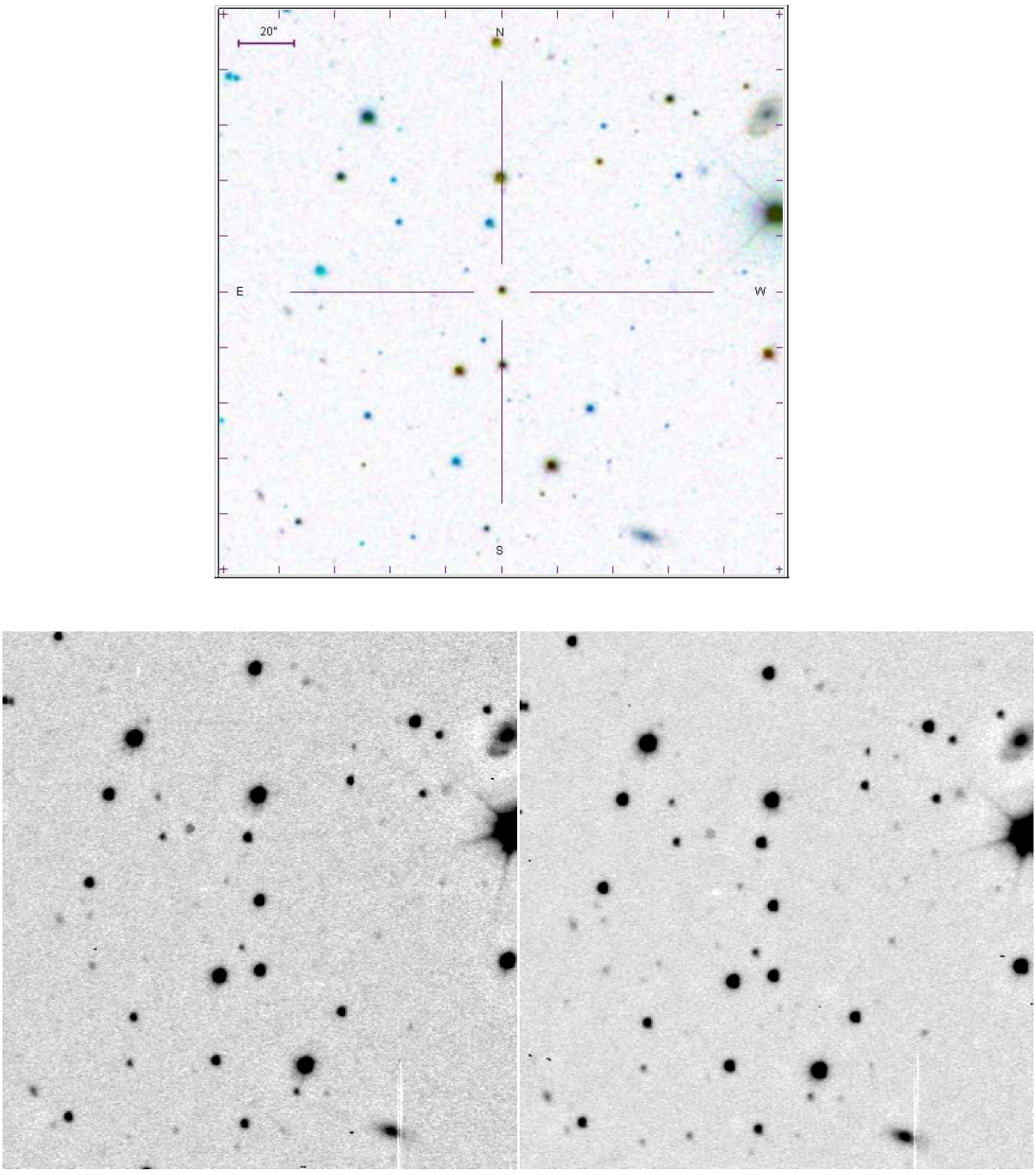

Figure 11: *Top:* The part of studied field from SDSS (combined *gri* image). Shown size is 3.38×3.38 arcsec. The total exposure time is ∼162s. FWHM is 1.44 arcsec for g-filter and 1.20 arcsec for r-filter. *Bottom:* About the same part of SALTICAM image in g-filter (left) and r-filter (right) after accurate flat-fielding. Exposure is 60s for each image. FWHM is ∼2.3 arcsec for each filter. The faintest objects, which are visible in g, possibly have ∼23.0 mag. The faintest objects, which are visible in r, possibly have ∼22.0 mag.

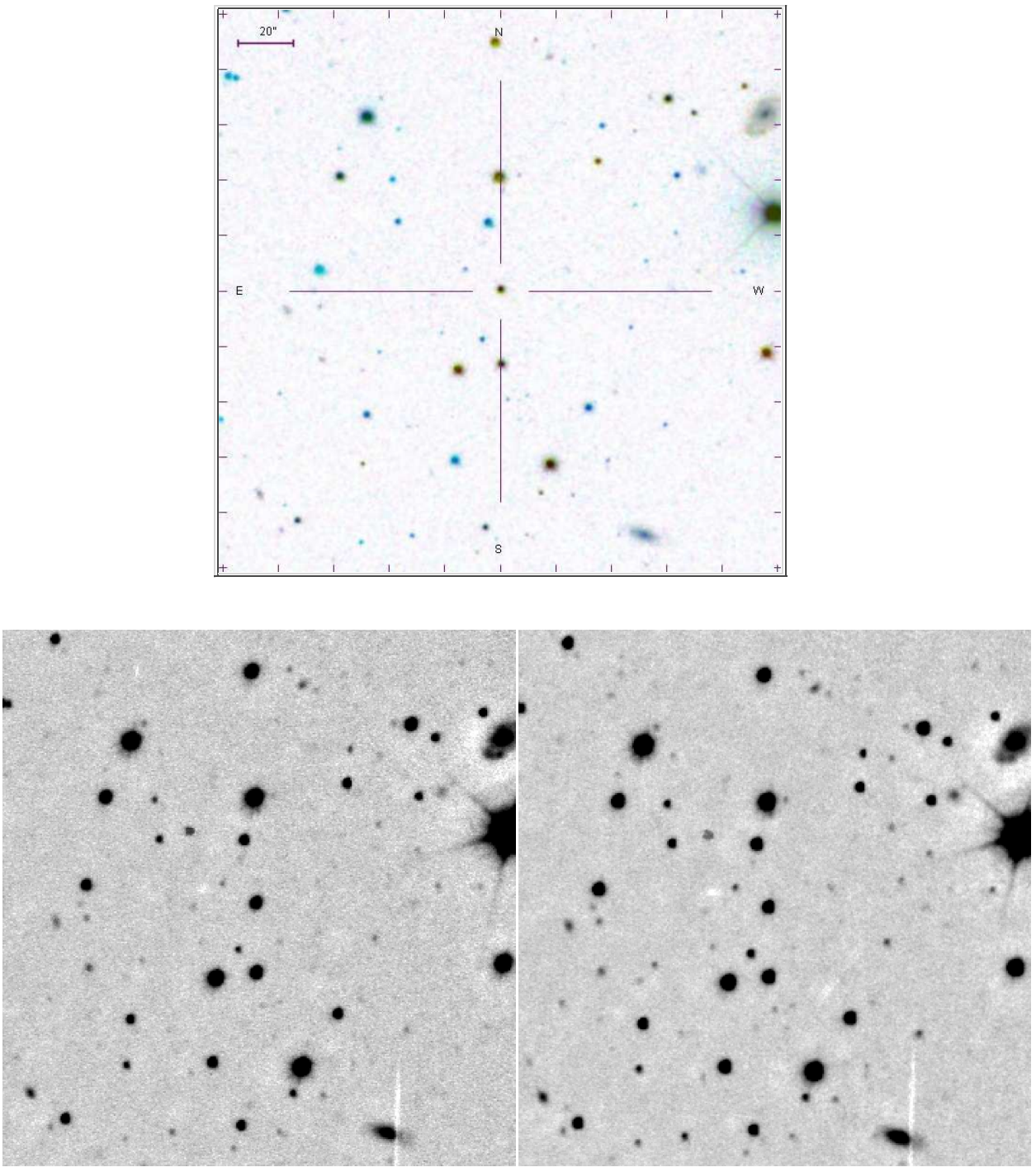

Figure 12: *Top:* The part of studied field from SDSS (combined *gri* image). Shown size is 3.38×3.38 arcsec. The total exposure time is ∼162s. FWHM is 1.44 arcsec for *g*-filter and 1.20 arcsec for *r*-filter. *Bottom:* About the same part of SALTICAM image in *g*-filter (left) and *r*-filter (right) after accurate flat-fielding and averaging of three frames in each filter. The total exposure is 180s for each filter. FWHM is ∼2.3 arcsec for each filter. It looks like the faintest visible objects are close to SDSS limits: g ∼23.5 mag and r ∼22.5 mag.

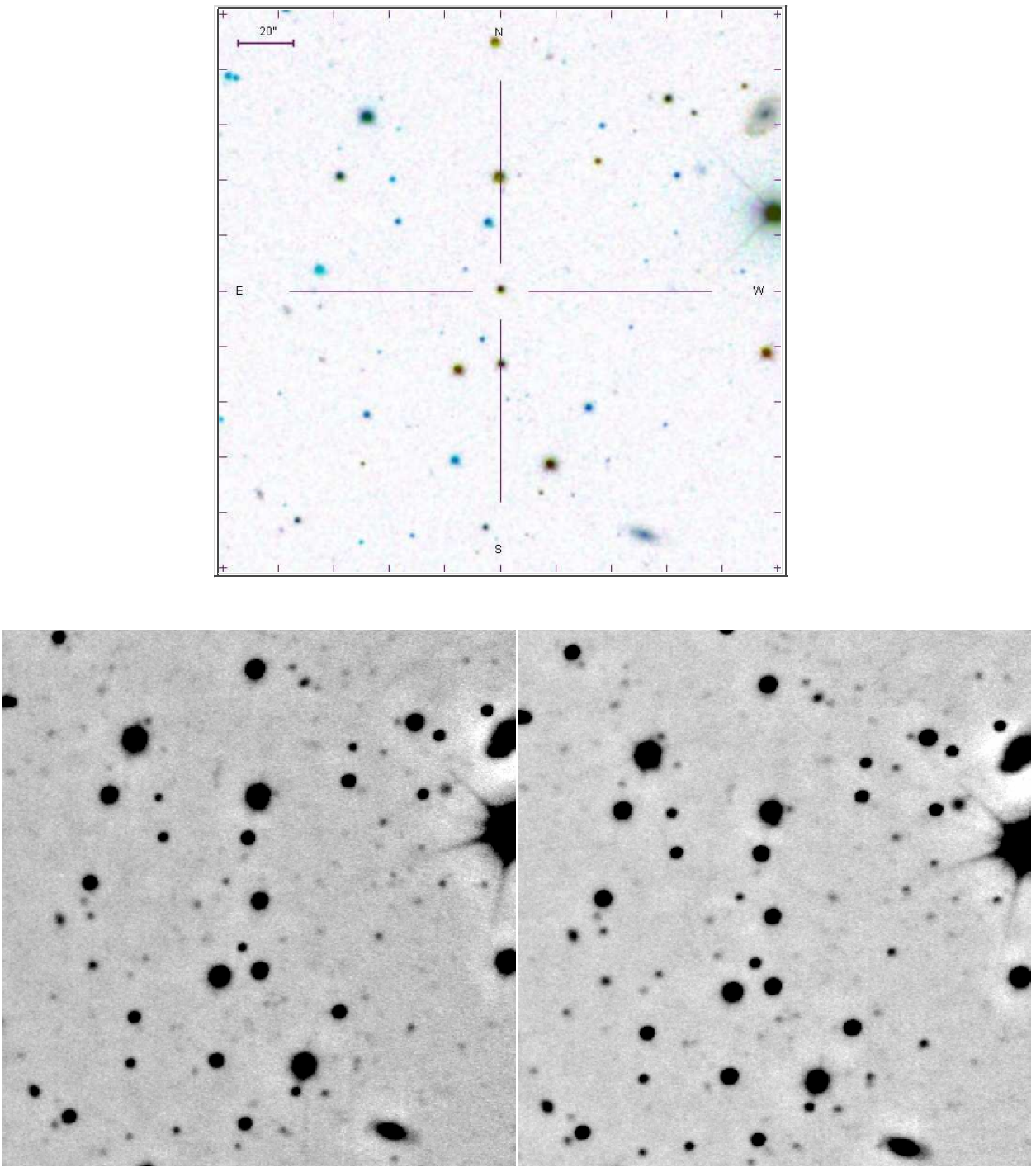

Figure 13: *Top:* The part of studied field from SDSS (combined *gri* image). Shown size is 3.38×3.38 arcmin. The total exposure time is ∼162s. FWHM is 1.44 arcsec for *g*-filter and 1.20 arcsec for *r*-filter. *Bottom:* About the same part of SALTICAM image in *g*-filter (left) and *r*-filter (right) after accurate flat-fielding and averaging of all 15 frames in each filter. The total exposure is 900s for each filter. The final FWHM is ∼2.7 arcsec for each filter. It looks like the faintest visible objects are fainter than on SDSS images.

4 Conclusions

As the result of this study we can produce some conclusions and observational recommendations:

1. The calculated average X, Y and rho drifts for the used azimuth coincide with previous measurements.

2. The exposure time of 60s per frame for g and r filters did not produce any significant elongation in these observations with seeing size about 2.3 arcsec on the frames.

3. Each dither of the telescope makes the image quality worse (the measured FWHM increases). Unfortunately, this way of observations (with no active or passive control of focus) does not give possibilities to correct for this effect.

4. A simple flat-field (use of all taken data to build an average illumination pattern) correction produces non-satisfactory final accuracy – the amplitude of sky background variations relative to the centre of the image can be up to 15%.

5. The suggested two step flat-fielding procedure results the final flatness of the sky background better than 1%.

6. The method used here of creating an illumination pattern for each observed frame works well only for not so crowded stellar fields and possibly does not work well for fields with very extended objects. Different kinds of combination of images might well help, however, and more accurate limitations have to be found in the future.

7. As a way to observe very extended objects with SALTICAM is to take separate sky fields for flat creation purposes with 10 arcmin offsets as part of the dither pattern.

References

Balona, Luis, 2007, SALT report, 1
Crawford S. M., et al., 2010, SPIE, 7737
Kniazev, A.Y. 2011, SALT report, **111111111**, 1 (in preparation)
Loaring, Nicola, 2006, SALT report, **2251AA0001**, 1
Loaring, Nicola, 2008, SALT report, **2251AA0003**, 1
Shergin, V.S., Kniazev, A.Y., & Lipovetsky, V.A., *New family of non-linear filters for background subtraction of wide-field surveys*, 1996, Astronomische Nachrichten, 2, 95
Vijay Mohan, 2011, SALT report, 1